# Supplemental Materials

***Molecular Biology of the Cell***

**Collins *et al*.**

**Supplementary Information**

# Microtubule number and nucleus-nucleus interactions uniquely regulate nuclear movement in muscle

Mary Ann Collins, L. Alexis Coon, Riya Thomas, Torrey R. Mandigo, Elizabeth Wynn, Eric S. Folker

**Fig. S1. Bocksbeutel, klarsicht, and ensconsin are necessary for proper muscle length and myonuclear position in *Drosophila* embryos.** (**A**) The average length of the lateral transverse muscles for the indicated genotypes. (**B–D**) Graphs indicating the raw distance between the dorsal end of the muscle and the nearest nucleus (**B**), the raw distance between the ventral end of the muscle and the nearest nucleus (**C**), and the raw distance between the dorsal and ventral nuclear clusters (**D**). (**E–F**) The relative distribution of all internuclear distances measured, represented as raw values (**E**) and as a function of muscle length (**F**). (**G–I**) Graphs indicating the area of nuclei located near the dorsal end of the muscle (**G**), the area of nuclei located near the ventral end of the muscle (**H**), and the total area of all myonuclei present within the muscle (**i**). It is important to note that in 21 out of the 27 $ens^{swo}$ embryos, there was only one cluster present. Thus, the dorsal cluster area was only measured in the 6 embryos that had two distinct clusters. Data points in (A–D) and (G–I) correspond to the average value within a single embryo. Error bars indicate the s.d. from ≥25 embryos for each genotype taken from at least three independent experiments. For (A) Student's t-test with Welsh's correction was used to assess the statistical significance of differences in measurements between experimental

genotypes to controls. For (B–D) and (G–I) One-way ANOVA with Tukey HSD post hoc test was used to assess the statistical significance of differences in measurements between all experimental groups.

**Fig. S2. Total nuclear volume and number of nuclei are not disrupted in *ensconsin*-depleted embryos.** (**A**) Three-dimensional volumetric renderings of nuclear clusters created from Airyscan images of a single LT muscle from stage 16 (16 hours AEL) control and $ens^{swo}$ embryos. Muscles in magenta, myonuclei in green. Scale bar, 5 µm. Each rendering showing just the nuclei have been rotated -90° (left) and +90° (right) along the y-axis as well as -90° (bottom) and +90° (top) along the x-axis, relative to the center image. (**B**) The number of nuclei per hemisegment counted from live stage 17 (17 hours AEL) control and $ens^{swo}$ embryos. Data points correspond to the total number of nuclei counted within a single hemisegment. Error bars indicate the s.d. from 40 hemisegments for each genotype taken from 10 different embryos. Student's t-test with Welsh's correction was used to assess the statistical significance of differences in the number of nuclei counted from $ens^{swo}$ embryos and controls. (**C**) The total volume of nuclei within a single LT muscle. Data points correspond to the total volume of nuclei within a single LT muscle. Error bars indicate the s.d. from 24 LT muscles for each genotype measured from six different embryos. Student's t-test with Welsh's correction was used to assess the statistical significance of differences in nuclear volume between $ens^{swo}$ embryos and controls.

**Fig. S3. *In vivo* 2-photon laser ablation of myonuclei within *Drosophila* embryos.** (**A**) Schematic illustrating how myonuclei are ablated in the lateral transverse (LT) muscles of a living stage 16 (16 hours AEL) control embryo. Nuclei (green) in the LT muscles (dotted grey outline) are identified by the expression of DsRed. Before ablation, all nuclei within a hemisegment are imaged. The nucleus to be ablated is selected by a region of interest (magenta ROI) and then ablated using a pulsed 2-photon laser at 860 nm for 1 s. The remaining

nuclei are then imaged every second for 30 s to observe the post-ablation response. (**B–C**) Montages from time-lapse images showing failed ablation attempts. Nuclei in green, transmitted light in gray. Photobleached nuclei were characterized by just the loss of fluorescence with no subsequent response (**B**) while embryos that were boiled were identified by a hole burned through the membrane (**C**, arrowhead). Scale bar, 5 μm. (**D**) Montage from a time-lapse image showing the ablation of a single nucleus within the LT muscles of a stage 16 control embryo. The first frame shows all the nuclei before the ablation event (0 s). The next frame (1 s) shows the ablation of a single nucleus (yellow circle), followed by the subsequent response of the remaining nuclei present within the cluster after the ablation event (white arrows). (**E**) Still images from a stage 16 embryo that was followed from the time of ablation until stage 17 (the final embryonic stage) to demonstrate that ablation does not affect embryonic development or viability. Scale bar, 10 μm.

**Fig. S4. Model of myonuclear movement during *Drosophila* embryonic muscle development.** In skeletal muscle, the active translocation of myonuclei (green) is dependent on the integrity of the nuclear envelope and the organization of the dynamic microtubule cytoskeleton as understood by the imaging of GFP-EB1. To achieve proper nuclear positioning, the two nuclear envelope proteins, bocksbeutel and klarsicht, facilitate the separation and distribution of nuclei into two distinct clusters of equal size by relieving associative interactions between neighboring nuclei. Since each myonucleus acts as a local microtubule organizing center, microtubules (gray) nucleate from the nuclear periphery (minus ends, −) and extend out (plus ends, +) to the cell cortex. These microtubules are able to generate force to pull their attached nuclei via ensconsin, which maintains the organization of the MT-network and promotes the sliding of adjacent microtubules. As a result of the coordinated actions of these

proteins, nuclei are pull to the end of the muscle before achieving their final position. Blue arrows denote the direction of net displacement (Δd) of nuclei.

**Table S1. Summary of P-values.** The following scale was used to determine statistical significance: not significant (ns) ≥ 0.05, *P<0.05, **P<0.01, ***P<0.001, ****P<0.0001, N/A not applicable.

**Table S2. Summary of Image Acquisition Settings.** Parameters listed for each microscope system used in this study.

**Movie S1. Volumetric imaging of myonuclei in the lateral transverse muscle of a control *Drosophila* embryo.**

Movie of a three-dimensional volumetric rendering of the dorsal and ventral nuclear clusters within a single LT muscle from a stage 16 (16 hours AEL) control embryo. Muscles in magenta, myonuclei in green. Scale bar, 5 µm. The LT muscle is rotated 360° along the x-axis and 360° along the y-axis.

**Movie S2. Volumetric imaging of myonuclei in the lateral transverse muscle of an *ens$^{swo}$* mutant embryo.**

Movie of a three-dimensional volumetric rendering of the nuclear cluster within a single LT muscle from a stage 16 (16 hours AEL) *ens$^{swo}$* embryo. Muscles in magenta, myonuclei in green. Scale bar, 5 µm. The LT muscle is rotated 360° along the x-axis and 360° along the y-axis.

**Movie S3. Nuclear migration in the lateral transverse muscle of a control *Drosophila* embryo.**

Time-lapse acquisition showing the migration of myonuclei within four lateral transverse (LT) muscles of a control embryo. Tracks correspond to the movement of individual nuclei within each cluster over the course of two hours. Time-lapse starts at stage 15 (15 hours AEL, t = 0 min), when nuclei have already separated into two distinct clusters. Each LT muscle has one dorsal cluster and one ventral cluster that migrate directionally to opposite ends of the muscle. At stage 16 (16 hours AEL), the dorsal and ventral clusters have reached their respective muscle pole, maximizing the distance between them. Scale bar, 10 µm.

**Movie S4. Altered nuclear migration in the lateral transverse muscle of a *bocks*$^{DP01391}$ mutant embryo.**

Time-lapse acquisition showing the migration of myonuclei within four lateral transverse (LT) muscles of a *bocks*$^{DP01391}$ mutant embryo. Tracks correspond to the movement of individual nuclei over the course of two hours. Time-lapse starts at stage 15 (15 hours AEL, t = 0 min), where a majority of nuclei failed to separate and remain clustered together in the ventral end of the muscle. Only two escaper nuclei separate from the ventral cluster and migrate directionally toward the dorsal muscle pole. Scale bar, 10 µm.

**Movie S5. Altered nuclear migration in the lateral transverse muscle of a *klar*$^{1}$ mutant embryo.**

Time-lapse acquisition showing the migration of myonuclei within four lateral transverse (LT) muscles of a *klar*$^{1}$ mutant embryo. Tracks correspond to the movement of individual nuclei over the course of two hours. Time-lapse starts at stage 15 (15 hours AEL, t = 0 min), where a majority of nuclei failed to separate and remain clustered together in the ventral end of the muscle. Only one escaper nucleus separates from the ventral cluster and migrates directionally toward the dorsal muscle pole. Scale bar, 10 µm.

**Movie S6. Altered nuclear migration in the lateral transverse muscle of an *ens*$^{swo}$ mutant embryo.**

Time-lapse acquisition showing the migration of myonuclei within four lateral transverse (LT) muscles of an *ens*$^{swo}$ mutant embryo. Tracks correspond to the movement of individual nuclei over the course of two hours. Time-lapse starts at stage 15 (15 hours AEL, t = 0 min). In each LT muscle, none of the nuclei separate and remain within a single cluster. Scale bar, 10 µm.

**Movie S7. *In vivo* 2-photon laser ablation of myonuclei in a control *Drosophila* embryo.**

Time-lapse acquisition showing the ablation of a myonucleus within the lateral transverse (LT) muscles of a stage 16 (16 hours AEL) control embryo. The first frame shows the nuclei before ablation (0 s). The next frame (1 s) shows the ablation of a single nucleus (yellow circle), followed by the subsequent response of the remaining nuclei after ablation (2-5 s). Myonuclei in green, transmitted light in gray. Scale bar, 10 µm.

**Movie S8. *In vivo* 2-photon laser ablation of myonuclei in a *bocks$^{DP01391}$* mutant embryo.**

Time-lapse acquisition showing the ablation of a myonucleus within the lateral transverse (LT) muscles of a stage 16 (16 hours AEL) *bocks$^{DP01391}$* mutant embryo. The first frame shows the nuclei before ablation (0 s). The next frame (1 s) shows the ablation of a single nucleus (yellow circle), followed by the subsequent response of the remaining nuclei after ablation (5-30 s). Myonuclei in green, transmitted light in gray. Scale bar, 10 µm.

**Movie S9. *In vivo* 2-photon laser ablation of myonuclei in a *klar$^{1}$* mutant embryo.**

Time-lapse acquisition showing the ablation of a myonucleus within the lateral transverse (LT) muscles of a stage 16 (16 hours AEL) *klar$^{1}$* mutant embryo. The first frame shows the nuclei before ablation (0 s). The next frame (1 s) shows the ablation of a single nucleus (yellow circle), followed by the subsequent response of the remaining nuclei after ablation (5-30 s). Myonuclei in green, transmitted light in gray. Scale bar, 10 µm.

**Movie S10. *In vivo* 2-photon laser ablation of myonuclei in an *ens*$^{swo}$ mutant embryo.**

Time-lapse acquisition showing the ablation of a myonucleus within the lateral transverse (LT) muscles of a stage 16 (16 hours AEL) *ens*$^{swo}$ mutant embryo. The first frame shows the nuclei before ablation (0 s). The next frame (1 s) shows the ablation of a single nucleus (yellow circle), followed by the subsequent response of the remaining nuclei after ablation (5-30 s). Myonuclei in green, transmitted light in gray. Scale bar, 10 µm.

**Movie S11. *In vivo* imaging of EB1 comet dynamics in the lateral transverse muscles of a control *Drosophila* embryo.**

Time-lapse acquisition of the lateral transverse muscles in a stage 16 (16 hours AEL) control embryo expressing EB1.eYFP. Time course, 60 s. Scale bar, 5 µm.

**Movie S12. *In vivo* imaging of EB1 comet dynamics in the lateral transverse muscles of an *ens*$^{swo}$ mutant embryo.**

Time-lapse acquisition of the lateral transverse muscles in a stage 16 (16 hours AEL) *ens*$^{swo}$ mutant embryo expressing EB1.eYFP. Time course, 60 s. Scale bar, 5 µm.

**Movie S13. *In vivo* imaging of EB1 comet dynamics in the dorsal oblique muscles of a control *Drosophila* embryo.**

Time-lapse acquisition of the dorsal oblique muscles in a stage 16 (16 hours AEL) control embryo expressing EB1.eYFP. Time course, 60 s. Scale bar, 5 µm.

**Movie S14. *In vivo* imaging of EB1 comet dynamics in the dorsal oblique muscles of an *ens*$^{swo}$ mutant embryo.**

Time-lapse acquisition of the dorsal oblique muscles in a stage 16 (16 hours AEL) *ens*$^{swo}$ mutant embryo expressing EB1.eYFP. Time course, 60 s. Scale bar, 5 µm.

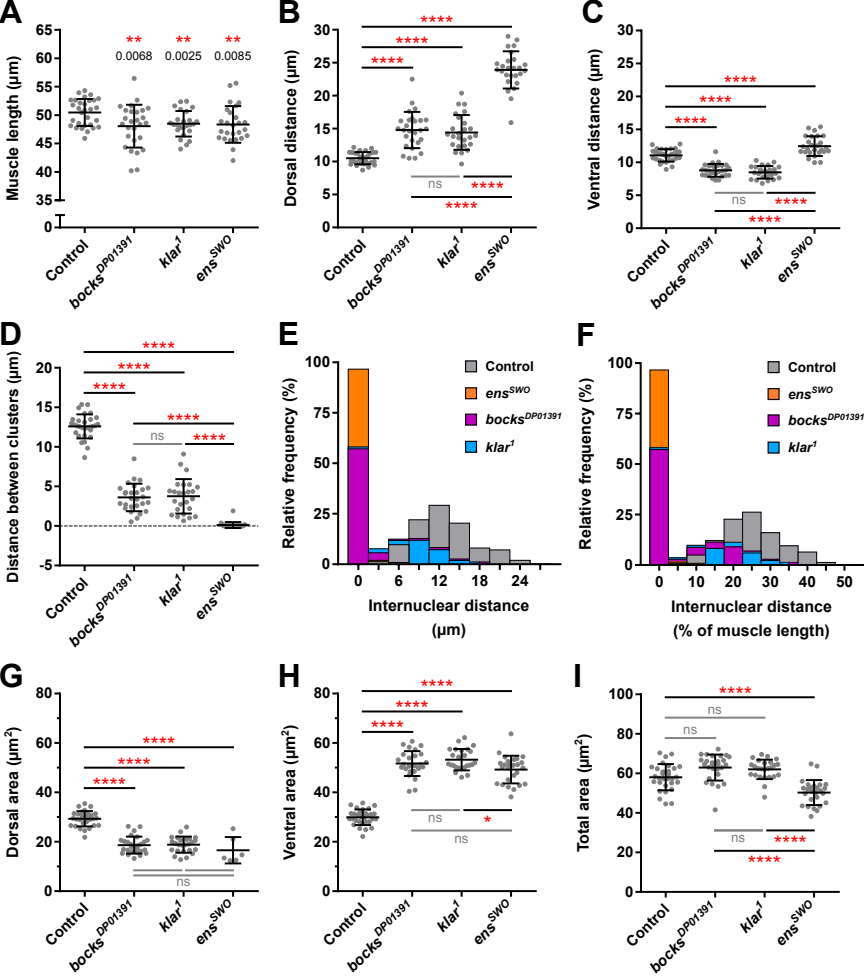


Collins et al., Figure S1

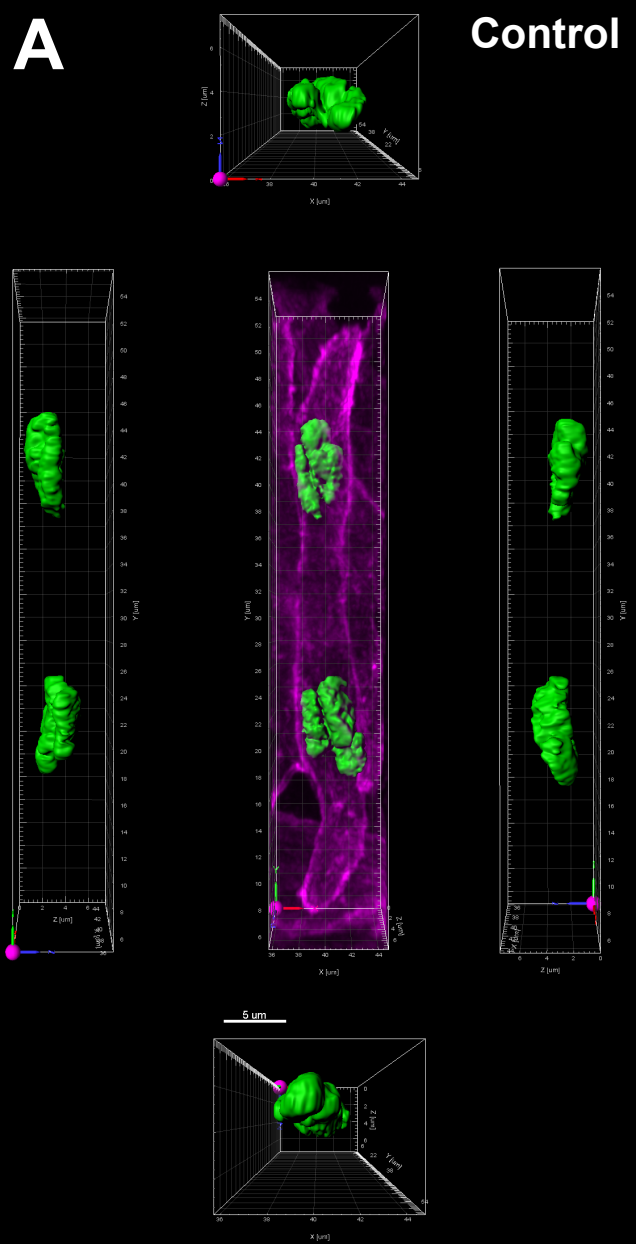


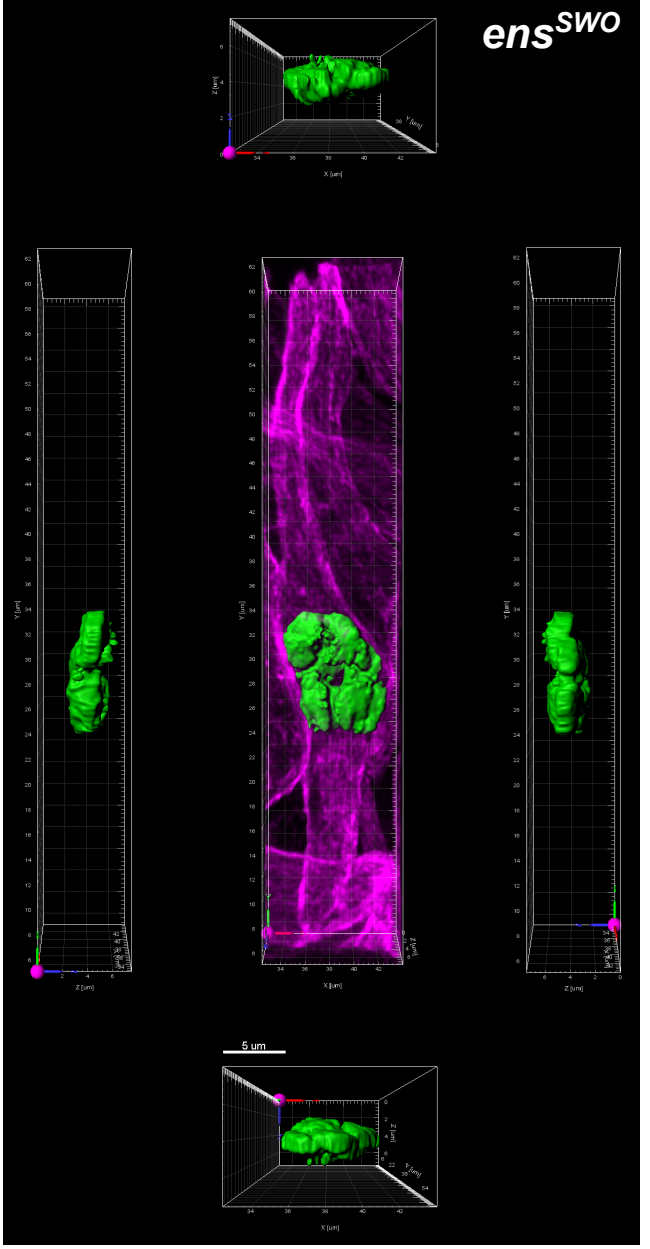


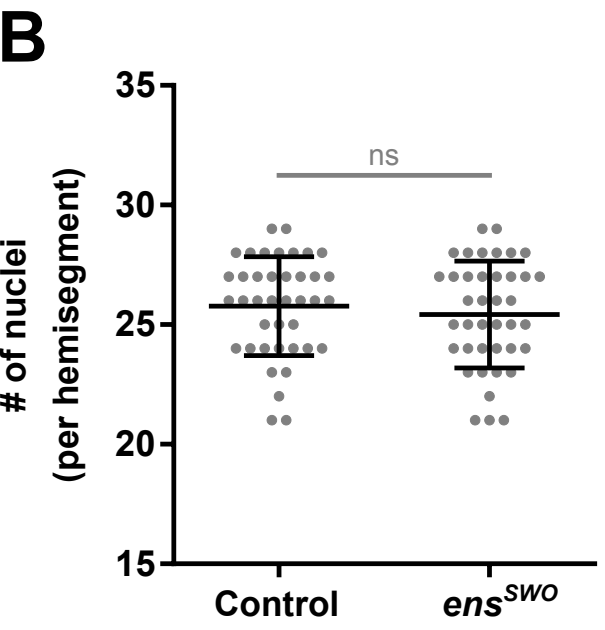


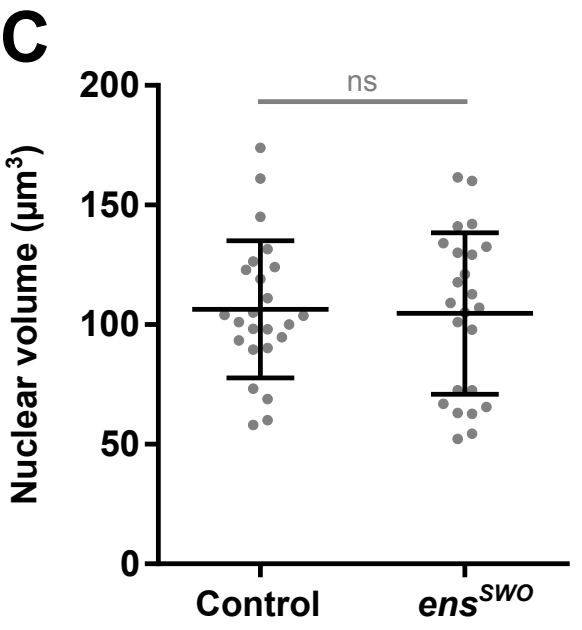


**Collins et al., Figure S2**

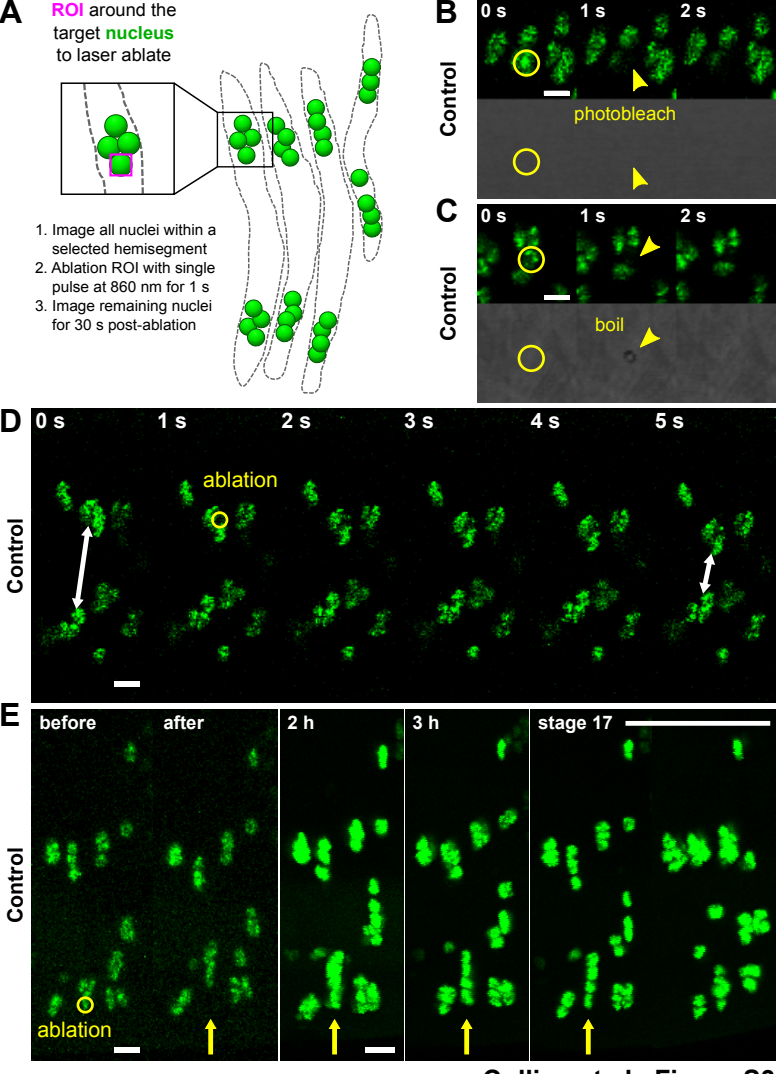


Collins et al., Figure S3

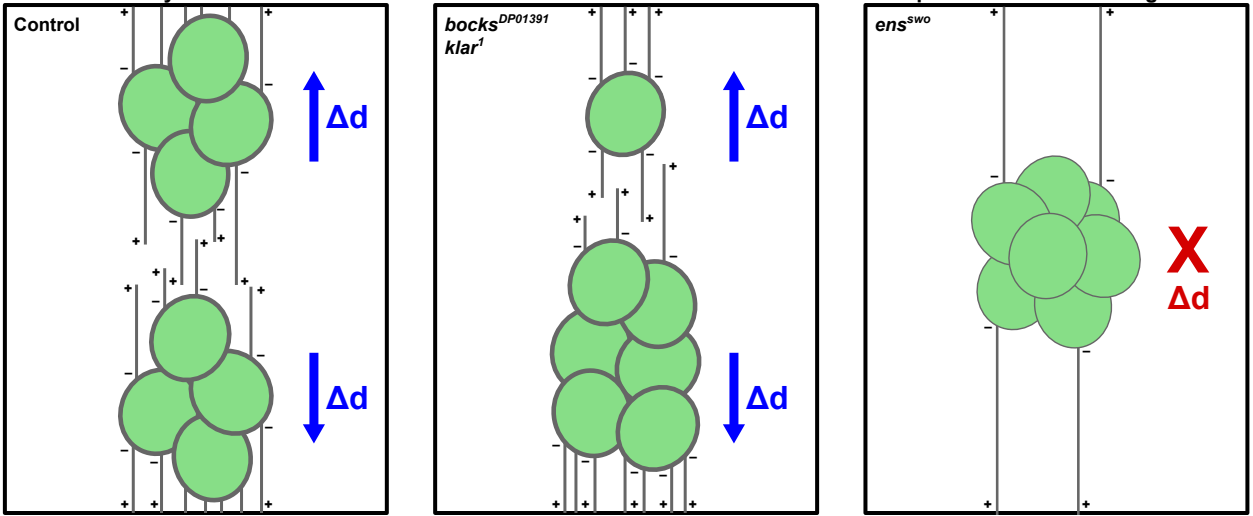


Collins et al., Figure S4

| Statistical Analysis | Genotype Comparisons: control vs. *bocks*$^{DP01391}$ | control vs. *klar*$^{1}$ | control vs. *ens*$^{SWO}$ | *bocks*$^{DP01391}$ vs. *klar*$^{1}$ | *bocks*$^{DP01391}$ vs. *ens*$^{SWO}$ | *klar*$^{1}$ vs. *ens*$^{SWO}$ |
|---|---|---|---|---|---|---|
| **Figure 1** (One-way ANOVA with Tukey HSD post hoc test) | | | | | | |
| **1B**: Dorsal distance (%) | **<0.0001** | **<0.0001** | **<0.0001** | 0.9858 | **<0.0001** | **<0.0001** |
| **1C**: Ventral distance (%) | **<0.0001** | **<0.0001** | **<0.0001** | 0.8985 | **<0.0001** | **<0.0001** |
| **1D**: Internuclear distance (%) | **<0.0001** | **<0.0001** | **<0.0001** | 0.9685 | **<0.0001** | **<0.0001** |
| **1E**: Nuclear separation ratio | **<0.0001** | **<0.0001** | **<0.0001** | 0.8120 | 0.9995 | 0.9142 |
| **Figure 2** (One-way ANOVA with Tukey HSD post hoc test) | | | | | | |
| **2B**: Separation speed | **0.0003** | **0.0029** | **<0.0001** | 0.9957 | **<0.0001** | **<0.0001** |
| **2D**: Ventral cluster aspect ratio | **<0.0001** | **<0.0001** | 0.9728 | 0.9200 | **<0.0001** | **<0.0001** |
| **2E**: Individual nuclear aspect ratio | **0.0327** | **0.0065** | **<0.0001** | 0.9416 | **<0.0001** | **<0.0001** |
| **2G**: Displacement | 0.3952 | 0.7351 | **<0.0001** | 0.0655 | **<0.0001** | **<0.0001** |
| **2H**: Nuclei that change direction | 0.0928 | 0.1242 | **<0.0001** | 0.9936 | **<0.0001** | **<0.0001** |
| **Figure 3** (One-way ANOVA with Tukey HSD post hoc test) | | | | | | |
| **3B**: Nuclear cluster area (before) | **0.0002** | **0.0002** | 0.1347 | >0.9999 | **0.0155** | **0.0134** |
| **3B**: Nuclear cluster area (after) | 0.0861 | 0.0851 | **0.0050** | >0.9999 | 0.4740 | 0.4783 |
| **3B'**: % change in cluster area | **<0.0001** | **<0.0001** | **0.0081** | 0.9989 | **<0.0001** | **<0.0001** |
| **3C'**: Total cluster displacement | **0.0004** | **0.0006** | **0.0044** | 0.9954 | **<0.0001** | **<0.0001** |
| **3D'**: Initial velocity (V0) | **0.0039** | **0.0342** | **0.0003** | 0.7175 | **<0.0001** | **<0.0001** |
| **Figure 4** (One-way ANOVA with Tukey HSD post hoc test) | | | | | | |
| **4E**: MT Distribution (AP:DV) | **<0.0001** | **<0.0001** | **<0.0001** | 0.8361 | **<0.0001** | **0.0002** |
| **Figure 5** (Student's t-test with Welsh's correction) | | | | | | |
| **5D**: EB1 comet velocity (LT muscles) | N/A | N/A | 0.4296 | N/A | N/A | N/A |
| **5D**: EB1 comet velocity (DO muscles) | N/A | N/A | 0.5967 | N/A | N/A | N/A |
| **5E**: # of EB1 comets (LT muscles) | N/A | N/A | **0.0024** | N/A | N/A | N/A |
| **5E**: # of EB1 comets (DO muscles) | N/A | N/A | **0.0094** | N/A | N/A | N/A |
| **Supplemental Figure 1** (*Student's t-test with Welsh's correction; One-way ANOVA with Tukey HSD post hoc test) | | | | | | |
| **S1A**: Muscle length* | **0.0068** | **0.0024** | **0.0085** | N/A | N/A | N/A |
| **S1B**: Dorsal distance (µm) | **<0.0001** | **<0.0001** | **<0.0001** | 0.9462 | **<0.0001** | **<0.0001** |
| **S1C**: Ventral distance (µm) | **<0.0001** | **<0.0001** | **<0.0001** | 0.7650 | **<0.0001** | **<0.0001** |
| **S1D**: Internuclear distance (µm) | **<0.0001** | **<0.0001** | **<0.0001** | 0.9878 | **<0.0001** | **<0.0001** |
| **S1G**: Dorsal area | **<0.0001** | **<0.0001** | **<0.0001** | 0.9980 | 0.5315 | 0.4700 |
| **S1H**: Ventral area | **<0.0001** | **<0.0001** | **<0.0001** | 0.6108 | 0.2171 | **0.0123** |
| **S1I**: Total area | 0.0519 | 0.0888 | **<0.0001** | 0.9477 | **<0.0001** | **<0.0001** |
| **Supplemental Figure 2** (Student's t-test with Welsh's correction) | | | | | | |
| **S2B**: Nuclear volume | N/A | N/A | 0.8487 | N/A | N/A | N/A |
| **S2C**: # of nuclei | N/A | N/A | 0.4689 | N/A | N/A | N/A |

| **Zeiss LSM 700** Figures | | Fluorescent tag | Laser line | laser excitation λ (nm) | laser emission λ (nm) | detector start λ (nm) | dectector end λ (nm) | detector gain (a.u.) | laser power (%) | pinhole size ($x10^{-4}$ m) |
|---|---|---|---|---|---|---|---|---|---|---|
| **1A**: myonuclei | (embryo, fixed) | Alexa Fluor 555 | Diode 555 | 555 | 585 | 560 | 800 | 390 - 430 | 1.0 | 33.606 |
| **1A**: tropomyosin | (embryo, fixed) | Alexa Fluor 488 | Diode 488 | 488 | 518 | 300 | 572 | 440 - 510 | 1.0 | 69.271 |
| **2A,E**: myonuclei | (embryo, live) | DsRed-NLS | Diode 555 | 555 | 585 | 560 | 800 | 530 - 650 | 1.0 | 69.849 |
| **4A**: myonuclei | (larvae, fixed) | Hoechst 33342 | Diode 405-5 | 405 | 435 | 300 | 510 | 630 - 690 | 0.5 | 69.849 |
| **4A-C**: α-Tubulin | (larvae, fixed) | Alexa Fluor 488 | Diode 488 | 488 | 518 | 300 | 530 | 510 - 580 | 1.0 | 69.849 |

| **Zeiss LSM 710 NLO** Figures | | Fluorescent tag | Laser line | laser excitation λ (nm) | laser emission λ (nm) | detector start λ (nm) | dectector end λ (nm) | detector gain (a.u.) | laser power (%) | pinhole size ($x10^{-4}$ m) |
|---|---|---|---|---|---|---|---|---|---|---|
| **3A, S3B-E**: myonuclei | (embryo, live) | DsRed-NLS | DPSS 561-10 | 561 | 610 | 560 | 650 | 540 - 630 | 2.0 - 2.5 | 42.579 - 43.557 |
| **S3B,C**: background | (embryo, live) | transmitted light | TL detector | - | - | - | - | 470 - 500 | - | - |
| **3A, S3B-E**: ablation **for laser cutting only* | (embryo, live) | - | Chameleon Ultra II fs pulsed-IR laser | - | 860 | - | - | - | 15.0 - 17.0 | - |

| **Zeiss LSM 800 (Airyscan)** Figures | | Fluorescent tag | Laser line | laser excitation λ (nm) | laser emission λ (nm) | detector start λ (nm) | dectector end λ (nm) | detector gain (a.u.) | laser power (%) | pinhole size ($x10^{-4}$ m) |
|---|---|---|---|---|---|---|---|---|---|---|
| **5A**: EB1 | (embryo, live) | EB1.eYFP | Argon | 488 | 515 | 510 | 560 | 750 | 2.0 | 59.660 |
| **S2A**: myonuclei | (embryo, fixed) | Alexa Fluor 555 | DPSS 561-10 | 561 | 595 | 560 | 650 | 520 - 550 | 2.0 | 48.251 |
| **S2A**: tropomyosin | (embryo, fixed) | Alexa Fluor 488 | Argon | 488 | 515 | 400 | 560 | 640 - 680 | 2.4 | 48.251 |